Applied Catalysis B: Environmental 121–122 (2012) 50–56

Contents lists available at SciVerse ScienceDirect

Applied Catalysis B: Environmental

journal homepage: www.elsevier.com/locate/apcatb

Facile route to prepare bimodal mesoporous γ-Al_2O_3 as support for highly active CoMo-based hydrodesulfurization catalyst

Xinmei Liu*, Xiang Li, Zifeng Yan

State Key Laboratory for Heavy Oil Processing and Key Laboratory of CNPC, China University of Petroleum, Qingdao 266555, China

ARTICLE INFO

Article history:
Received 5 January 2012
Received in revised form 19 February 2012
Accepted 26 March 2012
Available online 3 April 2012

Keywords:
Bimodal mesoporous alumina
Nanorod
Hydrodesulfurization catalyst
HDS activity

ABSTRACT

In the presence of polyethylene glycol (PEG), bimodal mesoporous nanorod γ-Al_2O_3 was successfully synthesized via hydrothermal method. The pore structure, crystal parameters and morphology of the alumina can be controlled by PEG. The more PEG can facilely induce the formation of bimodal mesoporous skeletal nanorod structure and lead to the relatively higher crystallinity to the alumina. This novel structure alumina result in the catalysts for hydrodesulfurization (HDS) possessing lower metal–support interaction and higher crystal phase dispersion. The nanorod structure of alumina contributes shorter crystallite length and higher staking degree to the catalysts. Of note is that there is apparently pore confinement effect on the HDS process. The catalysts with bimodal mesoporous structure indicate the higher HDS activity than that of catalyst with mono-modal structure.

1. Introduction

Sulfur-containing compounds present in transportation fuels are responsible for the severe atmospheric contamination [1]. The combustion of these sulfur compounds generates SOx, which will be converted to acid rain to cause the damage of the eco-environment. Moreover, SOx will also poison the catalyst for exhaust emission treatment. Thus, the use of ultra-clean fuels with a lower content of sulfur is impelled by stringent environmental regulations in recent years. The maximum sulfur in diesel fuel in US has been decreased to 15 ppm since 2006 [2] and in Europe to 10 ppm since 2009 [3]. To meet the strict regulatory specifications of fuel products and new emission specifications for the exhaust gases, ultra-deep hydrodesulfurization of fractional oil has become an important issue in the petroleum refinery processes. Many efforts have now been devoted to designing new hydrotreating catalysts with higher activity and selectivity for hydrodesulfurization (HDS) of refractory polyaromatic sulfur compounds, particularly alkylated dibenzothiophene [4–6]. The conventional HDS catalysts are composed of nanometric MoS_2 crystallites promoted by cobalt or nickel oxides on γ-Al_2O_3 support. Different approaches, such as tuning active phase, controlling promoters and tailoring the structure of supports [7–10], have been used to improve the catalyst performance for HDS. Development of novel supports has been paid more attention to recently because the HDS performance is strongly dependent on the physicochemical nature of the support [11–13]. So far, a large variety of materials such as γ-Al_2O_3 [14,15], SiO_2 [16], ZrO_2 [17,18], TiO_2 [19] and mesoporous materials [20–22], have been used as supports for HDS catalysts.

Alumina is the most widely used support of hydrorefining catalysts owing to its attractive mechanical properties, intrinsic acid-base characteristics and adjustable surface physicochemical properties [23]. However, traditional alumina possesses only textural porosity with low surface areas (less than 250 m^2/g) and broad pore size distributions, which significantly limits its catalytic activity. The bimodal pore structure of alumina has been noted as the key feature to develop a high effective catalyst for the HDS processes, where the smaller pores provide the high surface area to load the active species for HDS reactions and the larger pores provide the suitable space for bulky reactant and product molecules to diffuse in less resistance [24–26]. Inspired by the successful synthesis of surfactant-templated mesoporous alumina, the control synthesis of bimodal porous alumina in the presence of various templates has been attempted via hydrolysis of the aluminum secondary butylate [27–35]. However, this synthesis involved the usage of expensive organic aluminum precursor in the complicated and unfriendly routes. Thus, a facile and environment-friendly route to prepare the bimodal mesoporous γ-Al_2O_3 at a cheaper cost is more desirable to develop highly active HDS catalysts.

Therefore, the objectives of this research were to: (1) devise a proper way to prepare γ-Al_2O_3 support with desirable physicochemical properties, such as the bimodal mesopores and the high surface area; (2) assess the catalytic performance of MoCo-catalysts supported on as-prepared bimodal mesoporous γ-Al_2O_3.

* Corresponding author. Tel.: +86 0532 86983056; fax: +86 0532 86981787.
E-mail address: lxmei@upc.edu.cn (X. Liu).

0926-3373/$ – see front matter © 2012 Elsevier B.V. All rights reserved.
http://dx.doi.org/10.1016/j.apcatb.2012.03.024

We used polyethylene glycol (PEG) as the template and aluminum nitrate as the Al source. γ-Al_2O_3 with the bimodal mesopore was synthesized via a facile hydrothermal route. We found that the most active CoMo-based catalyst supported on the novelly structured γ-Al_2O_3 is able to remove 98.5% of sulfur from 4,6-dimethyldibenzothiophene under 260 °C, 2 MPa hydrogen pressure and with liquid hourly space velocity (LHSV) of 2 h^{-1}.

2. Experimental

2.1. Chemicals

PEG (MW = 20,000), ammonium molybdate (analytical reagent, AR), cobaltous nitrate (AR) and ammonium carbonate (AR) were purchased from Sinopharm Chemical Reagent Co. Ammonia (AR) and carbon bisulfide (AR) were purchased from Nanjing Chemical Reagents Co. Aluminium nitrate (AR) was purchased from Sinpeuo Fine Chemical Reagents Co. Cyclohexane (AR) was purchased from Tianjing Chemical Reagents Co. Toluene (AR) was purchased from Rionlon BoHua Pharmaceutical & Chemical Co., Ltd. 4,6-Dimethyldibenzothiophene (99.6%, 4,6-DMDBT) was synthesized using the procedure as described by Gilman and Jacoby [36]. All chemicals were used as received without any further purification. Deionized water was used in all experiments.

2.2. Synthesis of bimodal mesoporous γ-Al_2O_3

Typically, a certain amount of PEG was dissolved in 80 ml of aluminum nitrate ($Al(NO_3)_3{\cdot}9H_2O$, 1 M) to form a transparent solution. Then this mixed solution and 80 ml of ammonium carbonate ($(NH_4)_2CO_3$, 1.75 M) were added together to a beaker under vigorous Stirring. Concurrent flow process was used here in order to avoid heterogeneity of precipitate species. The resulting precipitate was transferred into a Teflon-lined stainless autoclave, which was kept at 100 °C for 24 h. After that the resulting product was washed with deionized water and dried at 80 °C for 48 h. Finally, the product was calcined at 550 °C for 4 h. The calcination temperature was raised at ramp rate of 2 °C/min. Based on the quantities of PEG, the samples were named as BMA-1 (0 g PEG2W), BMA-2 (8 g PEG2W), BMA-3 (16 g PEG2W) and BMA-4 (24 g PEG2W).

2.3. Synthesis of γ-alumina-supported CoMo-based catalyst

After extrusion of the supports, the catalysts with 15 wt.% MoO_3 and 4 wt.% CoO were prepared by simultaneous incipient wetness impregnation of aqueous solutions of $(NH_4)_6Mo_7O_{24}{\cdot}24H_2O$ and $Co(NO_3)_2{\cdot}6H_2O$. Then, the catalysts were dried overnight at 100 °C. Calcination was performed under a flow of air at 550 °C during 2 h. The catalysts were named as CoMo-BMA-x, where x = 1–4 according to the nomenclature applied for the different alumina. In addition, the reference CoMo-CA catalyst was prepared with commercial pseudo boehmite as support.

2.4. Characterization

X-ray diffraction (XRD) patterns were collected at a speed of 0.01° s^{-1} in a Bruker Axs diffractometer (Germany) with CuK radiation generated at 40 kV, 30 mA. Nitrogen adsorption–desorption isotherms were measured in a Micromeritics TRISTAR 3000 analyzer at 77 K. Specific surface area of the samples was calculated using the Brunauer–Emmett–Teller (BET) method. The pore size distribution (PSD) was derived from the desorption branches of the isotherms using the Barrett–Joyner–Halenda (BJH) method. Transmission electron microscopy (TEM) images were recorded on a JEOL JEM 2100 electron microscope operated at 200 kV. Thermogravimetric and differential scanning calorimeter (TG–DSC) analysis was conducted on a thermogravimetric analyzer, QMS 403C (NETZSCH, Germany), with an air flow rate of 30 ml/min at a heating rate of 20 °C/min. Temperature-programmed reduction (TPR) was carried out on ChemBET3000 with a thermal conductivity detector. The response of the thermal conductivity detector was recorded in a 5% H_2/Ar stream at the flow rate of 80 m/min, while temperature was increased to 1000 °C at the heating rate of 10 °C/min.

2.5. Catalytic activity assessment

The catalytic activity test for HDS of 4,6-DMDBT was carried out in a fixed-bed flow-type reactor with 5 ml of catalyst. Prior to the test, the oxide catalysts were sulfurized with 3 wt.% CS_2 in cyclohexane solution at 300 °C for 6 h under 2 MPa hydrogen pressure. Then 4,6-DMDBT at concentration of 0.5 wt.% in toluene was introduced at an H_2/oil ratio of 300/1 (v/v) and LHSV of 2 h^{-1}. After test at 260 °C for 5 h the outlet gases were analyzed by gas chromatography (Agilent 3800) and GC-mass spectrometry (Agilent 5973N/6890).

3. Results and discussion

3.1. Structural and morphological features of catalyst support

The XRD patterns shown in Fig. 1a indicate that all as-synthesized samples were ammonium aluminum carbonate hydroxide (AACH) compound with a nominal composition of

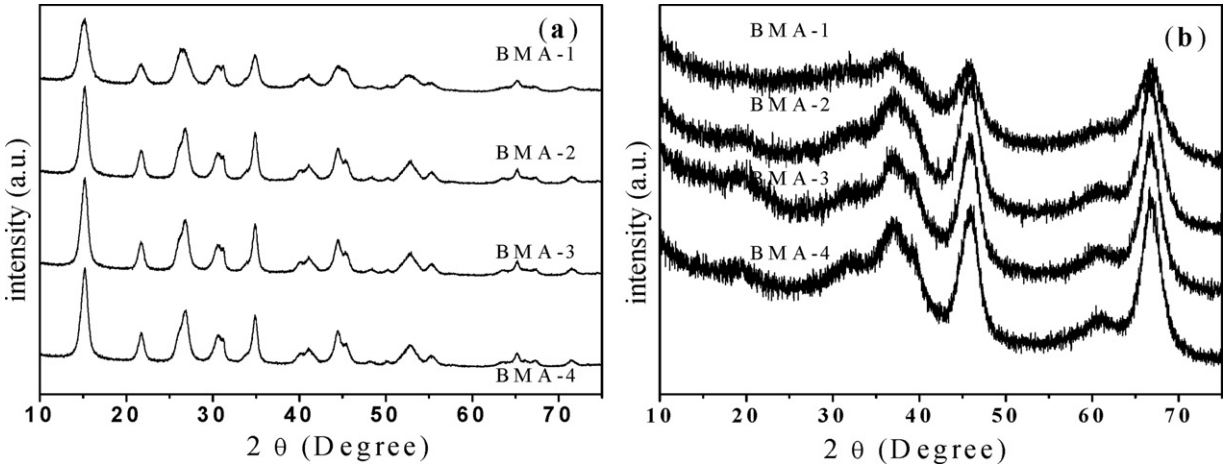

Fig. 1. XRD patterns of samples: (a) as-synthesized samples; (b) calcined samples.

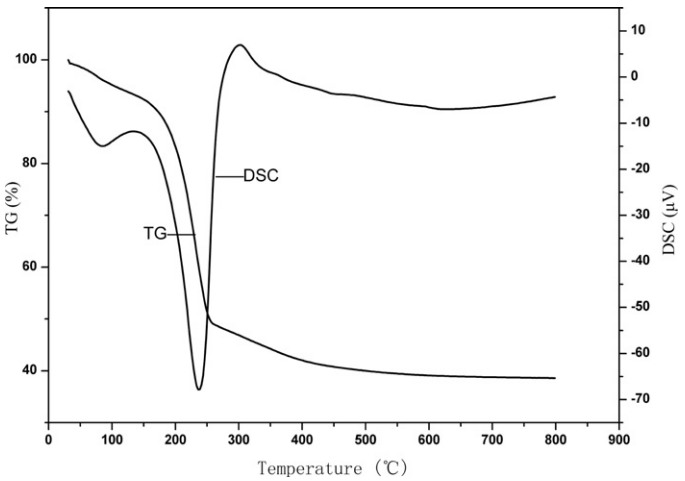

Fig. 2. TG–DSC plot of as-synthesized BMA-3 sample.

$NH_4Al(OH)_2CO_3$ (JCPDS card no. 42-0250). When more PEG2W was used in the synthesis, the peak intensity of as-prepared AACH was stronger. As investigated by Bai et al. [33] and Zhu et al. [39], high polymer molecules can selectively adsorb on certain faces of AACH crystals through hydrogen bonding and induce the crystal growth along some specific directions. Thus, the introduction of PEG into the synthesis system can promote the crystal growth. After calcination, all samples were converted to γ-Al_2O_3 phase (JCPDS card no. 10-0425) and the better crystallinity of as-obtained γ-Al_2O_3 seemed to inherit the better crystalinity of its precursor when more PEG was used.

As mentioned above, AACH was first prepared and then γ-Al_2O_3 was obtained upon thermal decomposition of AACH, which can be illustrated in the following reactions [37,38]:

$$Al(NO_3)_3 + 2(NH_4)_2CO_3 + H_2O \rightarrow NH_4Al(OH)_2CO_3\downarrow + 3NH_4NO_3 + CO_2\uparrow \quad (1)$$

$$NH_4Al(OH)_2CO_3 \rightarrow AlOOH + NH_3\uparrow + CO_2\uparrow + H_2O\uparrow \quad (2)$$

$$2AlOOH \rightarrow Al_2O_3 + H_2O\uparrow \quad (3)$$

Thermal gravimetry and differential scanning calorimeter (TG–DSC) profiles of as-synthesized BMA-3 sample are shown in Fig. 2. There were three weight loss stages in the TG curve. The first stage with the weight loss of 7.1% (check the loss at 150 °C) occurred at <150 °C, due to desorption of physically adsorbed water. The second one took place in the range of 150–250 °C, leading to 47.5% weight loss and being associated with the decomposition of AACH to form AlOOH (Eq. (2)). This weight loss process was also reflected by a strong endothermic peak at 235 °C in the DSC curve. The third weight loss (7.2%) occurred from 250 to 400 °C, which could be assigned to two processes. One was the burning of remnant polyethylene glycol, corresponding to the weak exothermic peak at 300 °C and the other was the phase transformation of AlOOH to γ-Al_2O_3, as presented in Eq. (3).

Table 1
Characteristics properties of bimodal mesoporous alumina and CoMo-based catalysts.

Sample	BET surface area (m^2/g)	Pore volume (cm^3/g)	Pore size (nm)
BMA-1	284.1	0.66	4.0, 15.4
BMA-2	333.6	0.95	3.4, 15.3
BMA-3	334.8	0.97	3.0, 11.2
BMA-4	494.7	1.02	2.7, 11.1
CoMo-BMA-1	204.2	0.38	3.9, 15.4
CoMo-BMA-2	280.8	0.74	3.3, 15.4
CoMo-BMA-3	283.1	0.75	2.9, 11.2
CoMo-BMA-4	400.3	0.81	2.6, 11.1
CoMo-CA	219.7	0.45	5.0

Nitrogen adsorption/desorption isotherms (see Fig. 3a) were typical of type V with two hysteresis loops, which means that as-obtained γ-Al_2O_3 samples were featured with the bimodal mesoporous structure. BJH pore size distribution (Fig. 3b) shows that the smaller pores were narrowly distributed in 2–5 nm while the larger ones exhibit a broad distribution (7–20 nm). As summarized in Table 1, the two pore diameters of the corresponding γ-Al_2O_3 were decreased and the total volume was apparently increased when more PEG was used in the precursor synthesis. As can be also noted in Table 1, the BET surface area was increased with the PEG amount used in the precursor preparation. These data demonstrate that PEG plays a key role in directing framework of AACH and the derived mesoporous alumina.

Fig. 4 illustrates the TEM images of as-obtained alumina samples. The BMA-1 mainly consisted of amorphous flakes (Fig. 4a). When PEG was involved in the precursor preparation, the derived alumina contained many nanorods with the diameter around of 4 nm (Fig. 4b–d). The number of nanorods seemed to increase with the PEG amount used in the preparation. The nanorods were randomly packed, irregularly forming some inter-particle voids. These voids seemed to corresponding to the larger mesopores detected

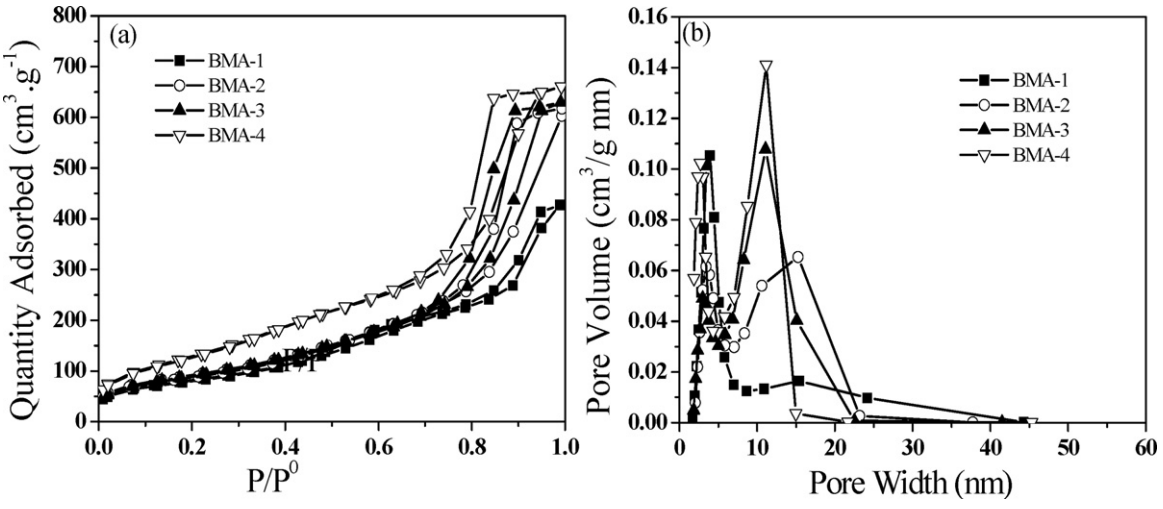

Fig. 3. N_2 adsorption isotherms (a) and BJH pore size distribution (b) of the alumina.

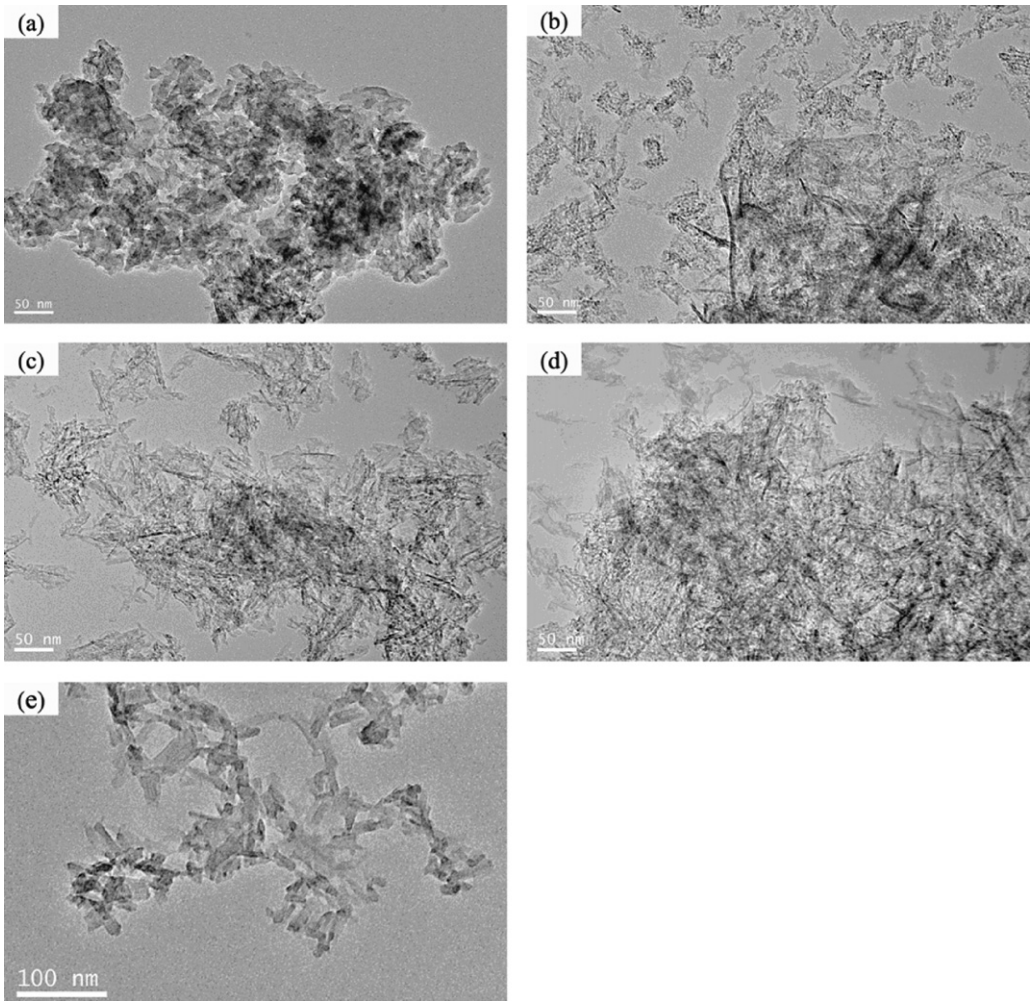

Fig. 4. TEM images of bimodal mesoporous alumina samples after calcination at 550 °C: (a) BMA-1; (b) BMA-2; (c) BMA-3; (d) BMA-4, and BMA-4 sample before calcination (e).

by the nitrogen adsorption. These morphological features suggest that [39,40] the rod-shaped micelles formed from PEG are selectively adsorbed on crystal faces of AACH via hydrogen bonding, which further induce the crystal growth into nanorods. With more and more PEG molecules adsorbed on the face of AACH crystals, the interaction between the particles becomes stronger and stronger, resulting in a close packing of the particles and increasing the pore size.

TEM images of as-synthesized and calcined BMA-4 are shown in Fig. 4d and e. As synthesized sample consisted of AACH crystals, which were loosely packed. After thermal decomposition of AACH crystals, small pores were generated due to the emission of gases such as NH_3, H_2O and CO_2 from the AACH framework. As shown in the TEM image of calcined BMA-4, such pores were "worm-like" mesopores, with the diameter of 1.7–4.5 nm.

3.2. Structural features and physicochemical properties of catalysts

The XRD patterns of as-prepared catalysts are shown in Fig. 5. For CoMo-BMA-1 and CoMo-CA samples, besides the peaks ascribed to γ-Al_2O_3, the signals of crystalline $CoMoO_4$ were identified in the range of $22^\circ < 2\theta < 30^\circ$. In contrast, no peaks of crystalline $CoMoO_4$ but very broad diffraction peaks of γ-Al_2O_3 were observed in other catalysts. This reveals that Co and Mo species are highly

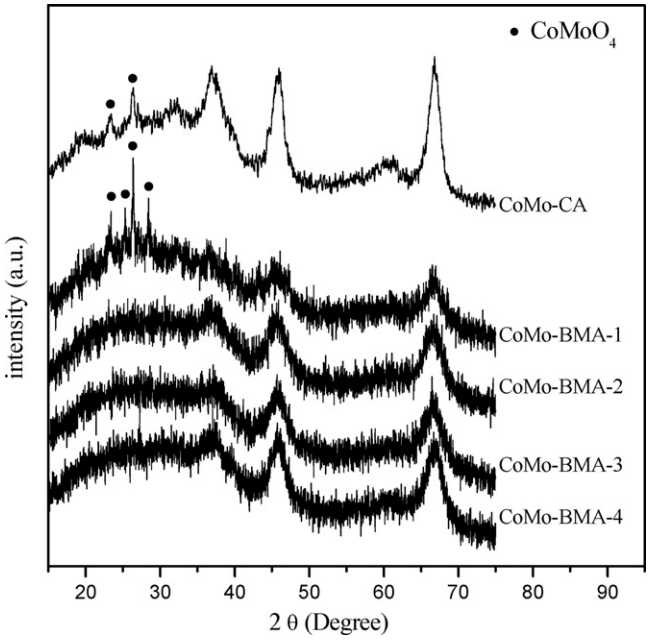

Fig. 5. XRD patterns of as-synthesized catalysts.

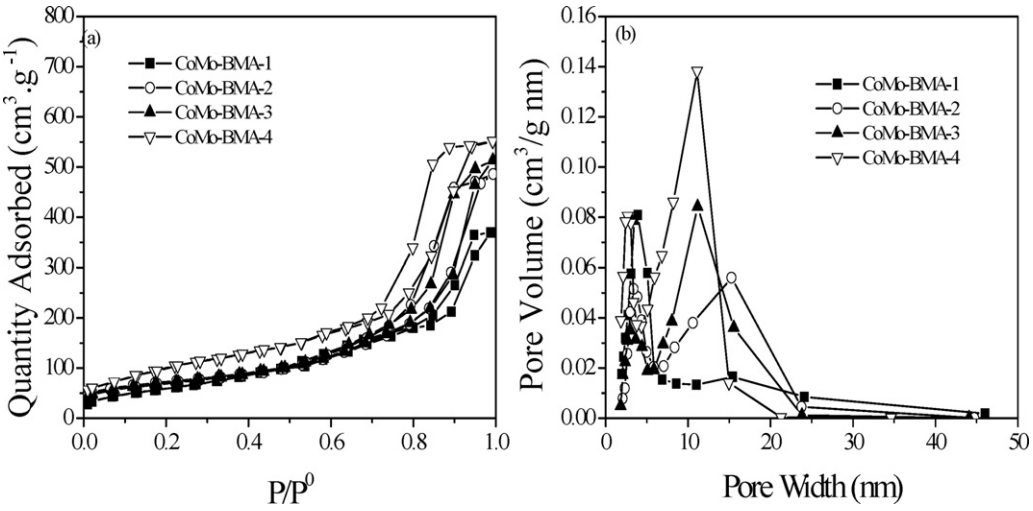

Fig. 6. N_2 adsorption isotherms (a) and BJH pore size distribution (b) of as-prepared catalysts.

dispersed over the alumina in these catalysts, which can be ascribed to the high surface area of the support.

The deposition of Co and Mo species resulted in the decrease of surface area and pore volume of the catalysts, as summarized in Table 1. Note that the bimodal pore structure was retained after deposition of the active components (Fig. 6b). The Co and Mo species were supposedly deposited on the surface of smaller mesopores. In compared of Fig. 3b with Fig. 6b, introduction of Co and Mo species decreased the smaller-pore volume while the larger-pore volume was nearly unchanged. In addition, the diameter of smaller pore was reduced but the larger one unchanged (Table 1). All these observations indicate that the Co and Mo species were mainly dispersed on the surface of the smaller mesopores. In contrast, the CoMo-CA catalyst prepared with commercial pseudo boehmite as the support had a mono-modal and broad pore distribution.

Fig. 7 illustrates TPR curves of the catalysts. Two peaks can be observed in range of 520–620 and 800–1000 °C for catalysts prepared with alumina obtained in the presence of PEG. The low-temperature peak is normally assigned to the reduction of octahedrally coordinated polymeric Mo species and the high-temperature peak to the reduction of tetrahedrally coordinated monomeric Mo species [41]. Because the first peak temperature in TPR profiles is related to the interaction between metal and support, Fig. 7 thus indicates that the metal–support interaction was decreased in the order of CoMo-BMA-1 > CoMo-BMA-2 ≈ CoMo-BMA-3 > CoMo-BMA-4. This order is inversely related to BET surface area of the catalyst. The higher surface area of the catalyst could allow Mo and Co oxide species to disperse more uniformly on the surface [42]. The higher dispersion of metal component and more bimodal mesopores promote the reduction of Mo species, thus decrease the reduction temperature. In addition, the peak at about 420 °C for CoMo-CA and CoMo-BMA-1 has been attributed to the reduction of bulk cobalt oxide [43], the absence of which in other catalysts further demonstrates the good dispersion of Co and Mo species.

HRTEM characterizations of sulfide CoMo-based catalysts were performed to examine the physical features of MoS_2 species. Fig. 8 shows the HRTEM micrographs of spent CoMo-CA and CoMo-BMA-2 catalysts. They mainly exhibited the edge or prism planes of MoS_2 slabs in these two catalysts. The MoS_2 slabs in catalyst CoMo-CA had an average stacking layer number of 1.83 with the average length of 3.42 nm, less in the stacking layer number but longer in the length than those of catalyst CoMo-BMA-2. The statistical parameters of these catalysts are listed in Table 2. Table 2 indicates that the average length of MoS_2 slabs was decreased in the order of CoMo-CA ≈ CoMo-BMA-1 > CoMo-BMA-2 > CoMo-BMA-3 > CoMo-BMA-4. The stacking layer number in catalysts CoMo-BMA-2, CoMo-BMA-3 and CoMoBMA-4 was obviously larger than that of CoMo-CA and CoMo-BMA-1. The length and layer number of MoS_2 slabs are two key factors determining the HDS performance, as these parameters are relevant to the active site [13,44]. The reports have showed that the active sites are mostly located on the edges and corners of the MoS_2 slabs. The shorter MoS_2 crystallite length and relative higher staking degree may have more active sites, and favor the HDS for highly refractory polyaromatic sulfur compounds.

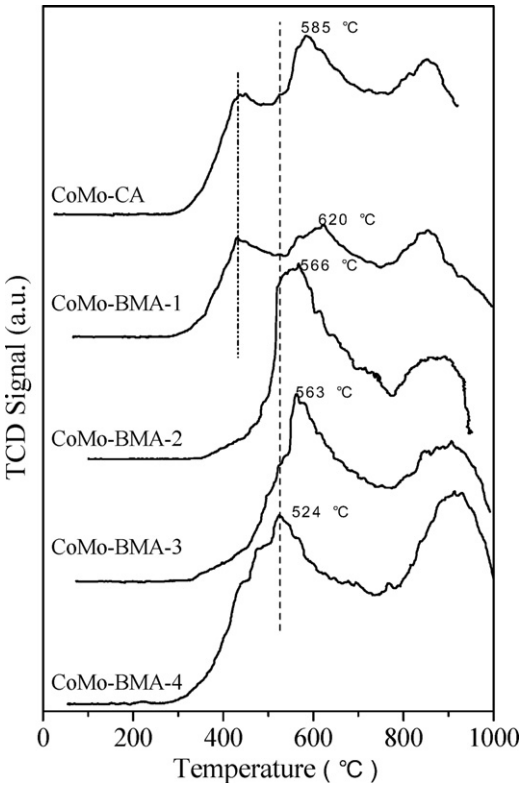

Fig. 7. Temperature-programmed reduction profiles of the CoMo-based catalysts.

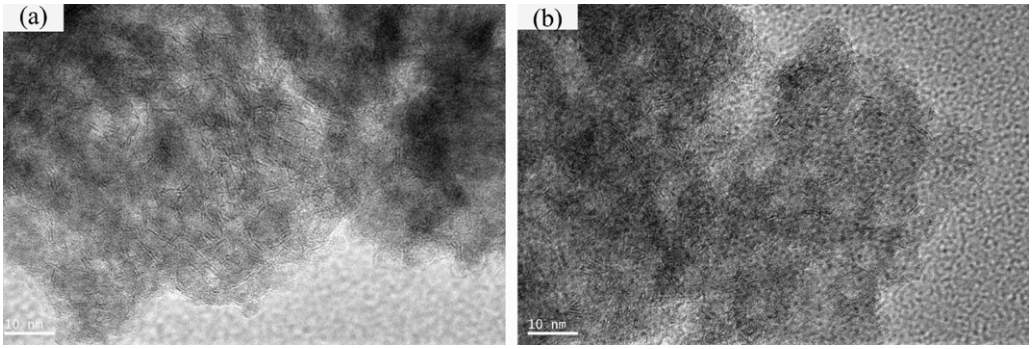

Fig. 8. HREM micrographs of MoS_2 crystallites observed with spent CoMo-CA (a) and CoMo-BMA-2 (b) catalysts.

Table 2
Structure of MoS_2 slabs, conversion and products distribution for the HDS of 4,6-DMDBT over different catalysts.

Catalyst	Average length (nm)	Stacking layer number	Products[a] (%)					Selectivity HYD/DDS ratio[b]	Conv. (%)[c]	Desulf. ratio (%)[d]
			4H	6H	DMBP	MCHT	DMBCH			
CoMo-CA	3.42	1.83	1.7	0.6	5.9	47.2	6.2	9.1	61.0	58.7
CoMo-BMA-1	3.55	1.78	1.1	–	5.3	55.3	6.4	11.61	68.1	67.0
CoMo-BMA-2	2.86	2.25	0.3	–	6.4	73.5	9.6	12.9	89.8	89.5
CoMo-BMA-3	2.84	2.22	0.2	0.1	7.0	75.7	10.3	12.3	93.4	93.1
CoMo-BMA-4	2.78	2.61	–	–	6.0	87.0	5.4	15.4	98.5	98.5

[a] 4H: tetrahydrodimethyldibenzothiophene (4HDMDBT); 6H: hexahydrodimethyldibenzothiophene (6HDMDBT); DMBP: dimethylbiphenyl; MCHT: methylcyclohexyltoluene; DMBCH: dimethylbicyclohexyl.
[b] Hydrogenation route (HYD) vs. direct desulfurization (DDS) route products: (MCHT + DMBCH)/DMBP.
[c] Conv. (%) = 4,6-DMDBT conversion (%) = 4H + 6H + MCHT + DMBCH + DMBP.
[d] Desulf. ratio (%) = Desulfurization ratio (%) = MCHT + DMBCH + DMBP.

3.3. Catalytic activity assessment

HDS data of 4,6-DMDBT over different catalysts are summarized in Table 2. MCHT was the most selective product, while DMBP and DMBCH were not highly but similarly selected for all catalysts. The HYD/DDS ratio (Table 2) indicates that dominant pathway of HDS over these catalysts was hydrogenation route. In particular, the MCHT selectivity over catalysts CoMo-BMA-2, CoMo-BMA-3 and CoMo-BMA-4 is much higher than that over catalysts CoMo-CA and CoMo-BMA-1, indicating the superior HDS activity of the former catalysts by the HYD route. The minor difference in DMBP selectivity over the catalysts is ascribed to the similar steric hindrance effect of 4,6-DMDBT on the DDS pathway [45].

Of note is that catalyst CoMo-BMA-1 with a smaller specific surface area than catalyst CoMo-CA (204 m^2/g vs. 220 m^2/g) exhibited a higher catalytic activity (68% vs. 61%), which implies that the catalyst supported on bimodal mesoporous alumina shows a better catalytic performance than that supported on mono-modal pore alumina. In the bimodal mesoporous alumina support, the larger mesopores probably enhance the diffusion rate of reactants and products, leading to the higher HDS activity of the catalyst. In a closer examination, we found that catalyst CoMo-BMA-3 had almost the same surface area and active phase dispersion to catalyst CoMo-BMA-2 (Table 1), but showed a higher HDS activity than CoMo-BMA-2 (Table 2), which could be attributed to the narrower pore size distribution. This thus demonstrates that the bimodal mesopore distribution is also important in effective sulfur removal. Remarkably, catalyst CoMo-BMA-4 showed an excellent performance, with the conversion and desulfurization ratio for 4,6-DMDBT up to 98.5%, much higher than that previously reported [46,47]. The highest catalytic performance of catalyst CoMo-BMA-4 could be attributed to the elegant combination of the mesopore structure (bimodal), the even dispersion of active MoS_2 species on the surface of small pores, and the layer number and the length of MoS_2 slabs.

4. Discussion

Although the similar PEG route for mesoporous alumina using aluminium nitrate is previously reported by Zhao et al. [48] and Zhu et al. [39], bimodal mesoporous structure was not obtained in their work. Also, the hydrothermal treatment temperature was either too low or too high to induce nanorod AACH crystal. In this research, the bimodal meoporous nanorod alumina can be obtained with suitable hydrothermal conditions. The addition of PEG to the synthesizing system of alumina can facilely induce crystal growth orienting along the PEG chain. The condensation of inorganic species along the organic chain results in the formation of nanorod structure. Of note is that more introduction of the PEG can not only improve the relative crystallinity of alumina, but also causes more nanorod as well as mesoporous structure exhibited in the samples.

The role played by nanocrystallite size and mesoporous structure is comparable, in some cases, to the chemical composition, adding another flexible parameter for designing and controlling the catalyst behavior [49]. The introduction of the bimodal meoporous nanorod alumina to the HDS catalyst can significantly improve the catalyst physical properties and reaction performance. The large surface area of the alumina contributes high dispersion of active phase to the catalysts. The less lattice defects for the samples with higher crystallinity leads to lower metal–support interaction, which further enhances the dispersion of active phase and facilitates the reduction of the metal catalyst at relative low temperature. The higher dispersion of active components means the higher HDS activity of the catalysts. Meanwhile, the nanorod structure of alumina results the catalyst possessing shorter crystallite

length and higher staking degree. The larger mesopores enhance the diffusion rate of reaction species and the smaller one supply the reacting sites. For a structure sensitive reaction, the above factors will be beneficial to the reaction performance.

5. Conclusion

In the presence of PEG, bimodal mesoporous nanorod γ-Al_2O_3 was successfully synthesized via hydrothermal approach. The relative crystallinity, the BET surface area and pore volume of alumina can be increased by introduction of PEG. The PEG molecules can be selectively adsorbed on certain faces of AACH crystals through hydrogen bonding and induce the crystal growth along the specific direction to give 1D nanorod morphology. The introduction of alumina with bimodal mesopore to the HDS catalysts can decrease the metal–support interaction, reduction temperature of molybdic oxide and diffusion resistance. It contributes the higher dispersion of active phase and more active sites to the catalysts. These cause that the CoMo-based catalysts prepared with bimodal mesoporous alumina have higher HDS activity for 4,6-DMDBT compared to the catalyst with mono-modal pores. Due to the steric hindrance effect of 4,6-DMDBT on the DDS pathway, the dominant HDS route in this study is HYD.

Acknowledgements

We are grateful to Dr. Y.Q. Xu for providing 4,6-DMDBT. We thank Mr. H.P. Wang for his kind helps in XRD analysis, and Dr. Y.B. Li for kind assistance in TEM experiments.

References

[1] I.V. Babich, J.A. Moulijn, Fuel 82 (2003) 607–631.
[2] Environmental Protection Agency, Federal Register 66 (2001) 5101–5150.
[3] Y. Yoshimura, M. Toba, H. Farag, K. Sakanishi, Catalysis Surveys from Asia 8 (2004) 47–60.
[4] C. Song, Catalysis Today 86 (2003) 211–263.
[5] C. Sentorun-Shalaby, S.K. Saha, X.L. Ma, C.S. Song, Applied Catalysis B: Environmental 101 (2011) 718–726.
[6] J.G. Park, C.H. Ko, K.B. Yi, J.-H. Park, S.-S. Han, S.-H. Cho, J.-N. Kim, Applied Catalysis B: Environmental 81 (2008) 244–250.
[7] S.J. Sawhil, K.A. Layman, D.R. Van Wyk, M.H. Engelhard, C. Wang, M.E. Bussell, Journal of Catalysis 231 (2005) 300–313.
[8] A. Montesinos-Castellanos, T.A. Zepeda, B. Pawelec, E. Lima, J.L.G. Fierro, A. Olivas, J.A.H. Reyes, Applied Catalysis A: General 334 (2008) 330–338.
[9] T.A. Zepeda, B. Pawelec, J.N. Díaz de León, J.A. de los Reyes, A. Olivas, Applied Catalysis B: Environmental 111–112 (2012) 10–19.
[10] M. Nagai, Applied Catalysis A: General 322 (2007) 178–190.
[11] J.A.R.V. Veen, E. Gerkema, A.M.V. der Kraan, P.A.J.M. Hendricks, H. Beens, Journal of Catalysis 133 (1992) 112–123.
[12] E. Myszka, J.R. Grzechowiak, G.V. Smth, Enegy and Fuels 3 (1989) 541–543.
[13] B. Nela, L. Christine, B. Pascal, L. Carole, R. Loic, P. Edmond, D. Franck, R. Sébastien, Chemistry of Materials 21 (2009) 522–533.
[14] J.H. Kwak, J.Z. Hu, D. Mei, C.W.W. Yi, D.H. Kim, C.H.F. Peden, L. Allard, J. Szanyi, Science 325 (2009) 1670–1673.
[15] J. Escobar, M.C. Barrera, J.A. Toledo, M.A. Corte s-Jacome, C. Angeles-Chavez, S. Nunez, V. Santes, E. Gomez, L. Diaz, E. Romero, J.G. Pacheco, Applied Catalysis B: Environmental 88 (2009) 564–575.
[16] K. Soni, B.S. Rana, A.K. Sinha, A. Bhaumik, M. Nandi, M. Kumar, G.M. Dhar, Applied Catalysis B: Environmental 90 (2009) 55–63.
[17] R.K. Kaila, A. Gutiérrez, A. Outi, I. Krause, Applied Catalysis B: Environmental 84 (2008) 324–331.
[18] O.Y. Guttierez, F. Perez, G.A. Fuentes, X. Bokhimi, T. Klimova, Catalysis Today 130 (2008) 292–301.
[19] Y. Saih, M. Nagata, T. Funamoto, Y. Masuyama, K. Segawa, Applied Catalysis A: General 295 (2005) 11–22.
[20] B. Pawelec, J.L.G. Fierro, A. Montesinos, T.A. Zepeda, Applied Catalysis B: Environmental 80 (2008) 1–14.
[21] D. Gulkova, Y. Yoshimura, Z. Vit, Applied Catalysis B: Environmental 87 (2009) 171–180.
[22] Z. Vit, H. Kmentova, L. Kaluza, D. Gulkova, M. Boaro, Applied Catalysis B: Environmental 108–109 (2011) 152–160.
[23] C. Misra, Industrial Alumina Chemicals, ACS Monograph 184, American Chemical Society, Washington, DC, 1986.
[24] X.M. Liu, H.X. Xue, X. Li, Z.F. Yan, Catalysis Today 158 (2010) 446–451.
[25] J. Yu, J.C. Yu, M.K.P. Leung, W. Ho, B. Cheng, X. Zhao, J. Zhao, Journal of Catalysis 217 (2003) 69–78.
[26] X. Li, D. Han, Y. Xu, X. Liu, Z. Yan, Materials Letters 65 (2011) 1765–1767.
[27] W.H. Deng, M.W. Toepke, B.H. Shanks, Advanced Functional Materials 13 (2003) 61–65.
[28] T.Z. Ren, Z.Y. Yuan, B.L. Su, Langmuir 20 (2004) 1531–1534.
[29] T.Y. Ma, X.J. Zhang, Z.Y. Yuan, Journal of Physical Chemistry C 113 (2009) 12854–12862.
[30] W.H. Deng, B.H. Shanks, Chemistry of Materials 17 (2005) 3092–3102.
[31] Z.Y. Yuan, T.Z. Ren, A. Azioune, J.J. Pireaux, B.L. Su, Chemistry of Materials 18 (2006) 1753–1767.
[32] Y. Tokudome, K. Fujita, K. Nakanishi, K. Miura, K. Hirao, Chemistry of Materials 19 (2007) 3393–3398.
[33] P. Bai, P.P. Wu, Z.F. Yan, X.S. Zhao, Microporous and Mesoporous Materials 118 (2009) 288–295.
[34] J.P. Dacquin, J. Dhainaut, D. Duprez, S. Royer, A.F. Lee, K. Wilson, Journal of the American Chemical Society 131 (2009) 12896–12897.
[35] S.W. Bian, Y.L. Zhang, H.L. Li, Yu, Y.Y.L. Song, W.G. Song, Microporous and Mesoporous Materials 131 (2010) 289–293.
[36] H. Gilman, A.L. Jacoby, Journal of Organic Chemistry 3 (1938) 108–119.
[37] F. Kara, G. Sahin, Journal of the European Ceramic Society 20 (2000) 689–694.
[38] Z. Wu, Y. Shen, Y. Dong, J. Jiang, Journal of Alloys and Compounds 467 (2009) 600–604.
[39] Z.F. Zhu, H. Liu, H.J. Sun, D. Yang, L.Y. Guo, Chemical Engineering Journal 155 (2009) 925–930.
[40] R. Ganguly, V.K. Aswal, P.A. Hassan, I.K. Gopalakrishnan, J.V. Yakhmi, Journal of Physical Chemistry B 109 (2005) 5653–5658.
[41] C.H. Papadopoulou, J. Vakros, H.K. Matralis, C.H. Kordulis, A. Lycourghiotis, Journal of Colloid Interface Sciences 261 (2003) 146–153.
[42] S.L. Gonzàlez-Cortés, T. Xiao, T. Lin, M.L.H. Green, Applied Catalysis A: General 302 (2006) 264–273.
[43] J. Vakros, C. Kordulis, A. Lycourghiotis, Langmuir 18 (2002) 417–422.
[44] D. Ferdous, A.K. Dalai, J. Adjaye, Applied Catalysis A: General 294 (2005) 80–91.
[45] O.Y. Gutiérrez, D. Valencia, G.A. Fuentes, T. Klimova, Journal of Catalysis 249 (2007) 140–153.
[46] C. Kwak, J.J. Lee, J.S. Bae, K. Choi, S.H. Moon, Applied Catalysis A: General 200 (2000) 233–242.
[47] P. Torres-Mancera, J. Ramirez, R. Cuevas, A. Gutiérrez-Alejandre, F. Murrieta, R. Luna, Catalysis Today 107–108 (2005) 551–558.
[48] R. Zhao, F. Guo, Y. Hu, H. Zhao, Microporous and Mesoporous Materials 93 (2006) 212–216.
[49] Z.L. Wang, J.S. Yin, Materials Science and Engineering A 286 (2000) 39–47.